Optical transmission between III-V chips on Si using photonic wire bonding

Zhichen Gu,[1,*] Tomohiro Amemiya,[2,3] Atsushi Ishikawa,[3,4] Takuo Hiratani,[1] Junichi Suzuki,[1] Nobuhiko Nishiyama,[1] Takuo Tanaka,[3,5] and Shigehisa Arai[1,2]

[1]Department of Electrical and Electronic Engineering, Tokyo Institute of Technology, Tokyo 152-8552, Japan
[2]Quantum Nanoelectronics Research Center, Tokyo Institute of Technology, Tokyo 152-8552, Japan
[3]RIKEN Metamaterials Laboratory, Saitama 351-0198, Japan
[4]Department of Electrical and Electronic Engineering, Okayama University, Okayama 700-8530, Japan
[5]Research Institute for Electronic Science, Hokkaido University, Hokkaido 001-0020, Japan
[*]gu.z.ab@m.titech.ac.jp

Abstract: Photonic wire bonding (PWB) was used to achieve flexible chip-scale optical interconnection as a kind of 3D-freeform polymer waveguide based on the two-photon polymerization of SU-8. First, the fabrication conditions of PWB were determined for the two-photon absorption process, and the coupling structure between PWB and III-V optical components was numerically simulated in order to obtain high coupling efficiency. Then, using PWB, chip-to-chip optical transmission was realized between laser and detector chips located on a common Si substrate. We fabricated a 2.5-μm-wide PWB with 1:3 aspect ratio between two optical chips of 140-μm gap and achieved a connection loss of approximately 10 dB.

OCIS codes: (130.5460) Polymer waveguides; (130.0130) Integrated optics.

References and links

1. H. Shinohara, "Broadband access in Japan: rapidly growing FTTH market," IEEE Commun. Mag. **43**(9), 72–78 (2005).
2. X. Lin, A. Hosseini, X. Dou, H. Subbaraman, and R. T. Chen, "Low-cost board-to-board optical interconnects using molded polymer waveguide with 45 degree mirrors and inkjet-printed micro-lenses as proximity vertical coupler," Opt. Express **21**(1), 60–69 (2013).
3. J. E. Bowers, D. Liang, A. Fang, H. Park, R. Jones, and M. Paniccia, "Hybrid silicon lasers: the final frontier to integrated computing," Opt. Photonics News **21**(5), 28–33 (2010).
4. M. Kada, "Development of functionally innovative 3D-integrated circuit (dream chip) technology/high- density 3D-integration technology for multifunctional devices," in *IEEE International Conference on 3D System Integration (3DIC)* (IEEE, 2009), pp. 1–6.
5. V. Suntharalingam, R. Berger, S. Clark, J. Knecht, A. Messier, K. Newcomb, D. Rathman, R. Slattery, A. Soares, C. Stevenson, K. Warner, D. Young, L.-P. Ang, B. Mansoorian, and D. Shaver, "A four-side tileable back illuminated, three-dimensionally integrated megapixel CMOS image sensor," in *IEEE Solid-State Circuits Conference Digest of Technical Papers (ISSCC)* (IEEE, 2009), pp. 38–39.
6. A. Fazzi, R. Canegallo, L. Ciccarelli, L. Magagni, F. Natali, E. Jung, P. Rolandi, and R. Guerrieri, "3-D capacitive interconnections with mono-and bi-directional capabilities," IEEE J. Solid-State Circuits **43**(1), 275–284 (2008).
7. K. Niitsu, Y. Shimazaki, Y. Sugimori, Y. Kohama, K. Kasuga, I. Nonomura, M. Saen, S. Komatsu, K. Osada, N. Irie, T. Hattori, A. Hasegawa, and T. Kuroda, "An inductive-coupling link for 3D integration of a 90 nm CMOS processor and a 65 nm CMOS SRAM," in *IEEE Solid-State Circuits Conference Digest of Technical Papers (ISSCC)* (IEEE, 2009), pp. 480–481.
8. A. W. Fang, E. Lively, Y.-H. Kuo, D. Liang, and J. E. Bowers, "A distributed feedback silicon evanescent laser," Opt. Express **16**(7), 4413–4419 (2008).
9. S. Stankovic, R. Jones, M. N. Sysak, J. M. Heck, G. Roelkens, and D. Van Thourhout, "1310 nm hybrid III-V/Si Fabry-Perot laser based on adhesive bonding," IEEE Photonics Technol. Lett. **23**(23), 1781–1783 (2011).
10. S. Keyvaninia, G. Roelkens, D. Van Thourhout, C. Jany, M. Lamponi, A. Le Liepvre, F. Lelarge, D. Make, G. H. Duan, D. Bordel, and J. M. Fedeli, "Demonstration of a heterogeneously integrated III-V/SOI single wavelength tunable laser," Opt. Express **21**(3), 3784–3792 (2013).
11. C. Zhang, S. Srinivasan, Y. Tang, M. J. R. Heck, M. L. Davenport, and J. E. Bowers, "Low threshold and high speed short cavity distributed feedback hybrid silicon lasers," Opt. Express **22**(9), 10202–10209 (2014).
12. S. Srinivasan, A. Arrighi, M. J. R. Heck, J. Hutchinson, E. Norberg, G. Fish, and J. E. Bowers, "Harmonically mode-locked hybrid silicon laser with intra-cavity filter to suppress supermode noise," IEEE J. Sel. Top. Quantum Electron. **20**(4), 1100208 (2014).

#242795 Received 12 Jun 2015; revised 12 Aug 2015; accepted 12 Aug 2015; published 17 Aug 2015

13. H. Duprez, A. Descos, T. Ferrotti, C. Sciancalepore, C. Jany, K. Hassan, C. Seassal, S. Menezo, and B. Ben Bakir, "1310 nm hybrid InP/InGaAsP on silicon distributed feedback laser with high side-mode suppression ratio," Opt. Express **23**(7), 8489–8497 (2015).
14. T. Shimizu, N. Hatori, M. Okano, M. Ishizaka, Y. Urino, T. Yamamoto, M. Mori, T. Nakamura, and Y. Arakawa, "High density hybrid integrated light source with a laser diode array on a silicon optical waveguide platform for inter-chip optical interconnection," in *IEEE 8th International Conference on Group IV Photonics (GFP)* (IEEE, 2011), pp. 181–183.
15. G. Roelkens, L. Liu, D. Liang, R. Jones, A. Fang, B. Koch, and J. Bowers, "III-V/silicon photonics for on-chip and intra-chip optical interconnects," Laser Photonics Rev. **4**(6), 751–779 (2010).
16. M. J. R. Heck, J. F. Bauters, M. L. Davenport, J. K. Doylend, S. Jain, G. Kurczveil, S. Srinivasan, Y. Tang, and J. E. Bowers, "Hybrid silicon photonic integrated circuit technology," IEEE J. Sel. Top. Quantum Electron. **19**(4), 6100117 (2013).
17. N. Lindenmann, G. Balthasar, D. Hillerkuss, R. Schmogrow, M. Jordan, J. Leuthold, W. Freude, and C. Koos, "Photonic wire bonding: a novel concept for chip-scale interconnects," Opt. Express **20**(16), 17667–17677 (2012).
18. C. Koos, J. Leuthold, W. Freude, N. Lindenmann, S. Koeber, G. Balthasar, J. Hoffmann, T. Hoose, P. Huebner, D. Hillerkuss, and R. Schmogrow, "Photonic wire bonding: connecting nanophotonic circuits across chip boundaries," Proc. SPIE **8613**, 86130W (2013).
19. Z. Gu, T. Amemiya, A. Ishikawa, J. Kang, T. Hiratani, Y. Hayashi, J. Suzuki, N. Nishiyama, T. Tanaka, and S. Arai, "Investigation of optical interconnection by using photonic wire bonding," J. Laser Micro/Nanoeng. **10**(2), 148–153 (2015).
20. T. Shindo, M. Futami, K. Doi, T. Amemiya, N. Nishiyama, and S. Arai, "Design of lateral current injection type membrane distributed-feedback lasers for on-chip optical interconnections," IEEE J. Sel. Top. Quantum Electron. **19**(4), 1502009 (2013).
21. T. Shindo, T. Koguchi, M. Futami, K. Doi, Y. Yamahara, J. Lee, T. Amemiya, N. Nishiyama, and S. Arai, "10 Gbps operation of top air-clad lateral junction waveguide-type photodiodes," Jpn. J. Appl. Phys. **52**(11R), 118002 (2013).
22. D. Inoue, J. Lee, K. Doi, T. Hiratani, Y. Atsuji, T. Amemiya, N. Nishiyama, and S. Arai, "Room-temperature continuous-wave operation of GaInAsP/InP lateral-current-injection membrane laser bonded on Si substrate," Appl. Phys. Express **7**(7), 072701 (2014).
23. K. Doi, T. Shindo, J. Lee, T. Amemiya, N. Nishiyama, and S. Arai, "Thermal analysis of lateral current injection membrane distributed feedback laser," IEEE J. Quantum Electron. **50**(5), 321–326 (2014).
24. T T. Shindo, T. Okumura, H. Ito, T. Koguchi, D. Takahashi, Y. Atsumi, J. Kang, R. Osabe, T. Amemiya, N. Nishiyama, and S. Arai, "Lateral-current-injection distributed feedback laser with surface grating structure," IEEE J. Sel. Top. Quantum Electron. **17**(5), 1175–1182 (2011).
25. C. B. Schaffer, A. Brodeur, J. F. García, and E. Mazur, "Micromachining bulk glass by use of femtosecond laser pulses with nanojoule energy," Opt. Lett. **26**(2), 93–95 (2001).
26. Y. Liu, D. D. Nolte, and L. J. Pyrak-Nolte, "Large-format fabrication by two-photon polymerization of SU-8," Appl. Phys., A Mater. Sci. Process. **100**(1), 181–191 (2010).
27. G. P. Agrawal and N. K. Dutta, *Semiconductor Lasers* (Springer, 1993).

1. Introduction

Since the widespread usage of optical fibers in the 1980s for realizing intercontinental data transmission, optical communication systems have been continuously refined toward short-range applications such as household fiber-to-the-home (FTTH) and even smaller board-to-board interconnections in computing systems [1, 2]. Now, substantial efforts are focused in the field of intra-chip optical interconnects [3].

Because of excessive delays in long wires and high power consumption in large-scale integrated circuits (LSIs), many research groups have continued to explore new solutions for interconnecting functional blocks. Along with three-dimensional integrated circuits using through-silicon via (TSV) [4, 5], wireless capacitive and inductive couplings [6, 7] as well as optical interconnects have been considered to be promising solutions that provide a significant improvement in performance and power savings over copper-based solutions in conventional LSIs.

From the perspective of CMOS technology, photonic integration of various optical functionalities in a silicon-on-insulator (SOI) platform is being focused upon for intra-chip optical interconnects. However, the realization of light sources in an SOI platform remains

#242795 Received 12 Jun 2015; revised 12 Aug 2015; accepted 12 Aug 2015; published 17 Aug 2015

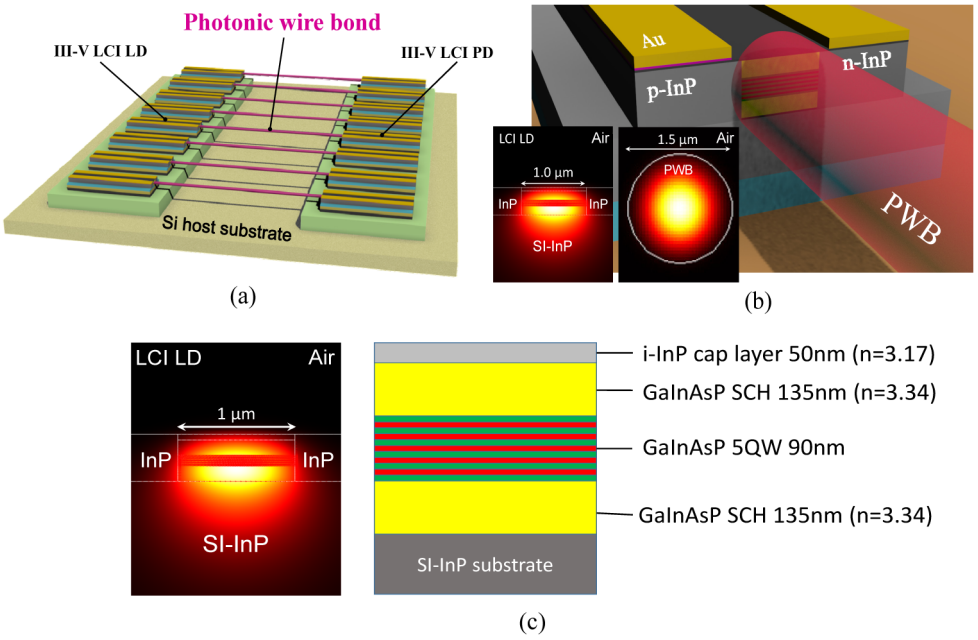

Fig. 1. (a) Concept of inter-chip optical interconnection between two lateral-current-injection (LCI) optical chips based on photonic wire bonding (PWB). (b) Details of the transition section between a polymer PWB waveguide and an LCI-FP laser, together with their mode profiles. (c) The enlarged modal intensity distribution of the core layer of LCI-FP laser and its cross-sectional structure.

challenging because Si is a poor light-emitting material because of its indirect energy bandgap. To overcome this problem, the integration of III-V components on Si, called hybrid integration, has been used as it merges direct-bandgap materials with low-loss Si passive waveguides [8–13].

Recent studies of hybrid integration primarily focus on two types of methods. One is the realization of a butt-coupling structure based on flip-chip bonding technology [14]. The designation of the coupling structure is very simple, while a relatively tight alignment would be necessary during the fabrication process for achieving low coupling loss. Moreover, the reflection between Si waveguides and lasers would also need to be suppressed. The other method is the heterogeneous integration based on the direct wafer bonding of a III-V material on a patterned silicon-on-insulator (SOI) substrate. To realize sufficient coupling between III-V light sources and Si waveguides, a device has to be designed carefully to have smooth mode transition by introducing taper structures [15, 16].

In the present paper, an emerging technology, named photonic wire bonding (PWB), was introduced as another solution to the III-V/Si hybrid integration. As the counterpart of the wire bonding technology in an electrical field, PWB allows efficient connection between arbitrary optical components as a kind of 3D-freeform polymer waveguide fabricated with a two-photon process [17–19]. For instance, it is possible to transfer light efficiently from the III-V region to the Si waveguides through PWB while maintaining the performance of the III-V light sources. We realized direct optical interconnection between a GaInAsP/InP lateral-current-injection (LCI) laser and photodiode [20, 21] on a Si wafer through benzocyclobutene (BCB) adhesive bonding and achieved 140-μm optical transmission via PWB with a connection loss of approximately 10 dB.

#242795 Received 12 Jun 2015; revised 12 Aug 2015; accepted 12 Aug 2015; published 17 Aug 2015

2. Numerical simulation

In order to realize heterogeneous photonic integration based on PWB, the optical signal is expected to have been emitted from an efficient III-V compound light source and have passed through the connected PWB, then coupled to low-loss passive components such as Si waveguides on an SOI platform, and finally detected using a high-sensitivity photodiode. As an initial step, PWB is considered to be used to realize direct optical transmission between two III-V optical components on a Si substrate, Fig. 1(a). The LCI laser chosen in this study was developed by our group to satisfy the demand for an ultralow-power-consumption light source in terms of on-chip optical interconnection; it consists of a thin semiconductor core layer sandwiched by air and semi-insulator InP (n = 3.17) claddings [22, 23]. Thus, the optical confinement factor in the active region of the LCI laser is approximately three times that of conventional double-heterostructure lasers because of the high index contrast between the core and upper air cladding, which leads to a lower-threshold-current operation.

The coupling loss between the PWB and other optical components such as the III-V LCI laser (or detector) is considered an essential factor of this technology. The designed end-face-contact coupling structure between the PWB and LCI laser and their mode profiles are shown in Fig. 1(b). The cross-sectional structure of the core layer of the laser and its enlarged modal intensity distribution are shown in Fig. 1(c), which shows an asymmetrical shape because the semi-insulating InP substrate has a higher refractive index than the upper air cladding. Here, SU-8 (n = 1.57 at 1550 nm) was chosen as the polymer material of the PWB for two-photon polymerization, and it is assumed that the structure of the GaInAsP/InP LCI Fabry–Pérot (FP) laser is the same as that of our previous device [24].

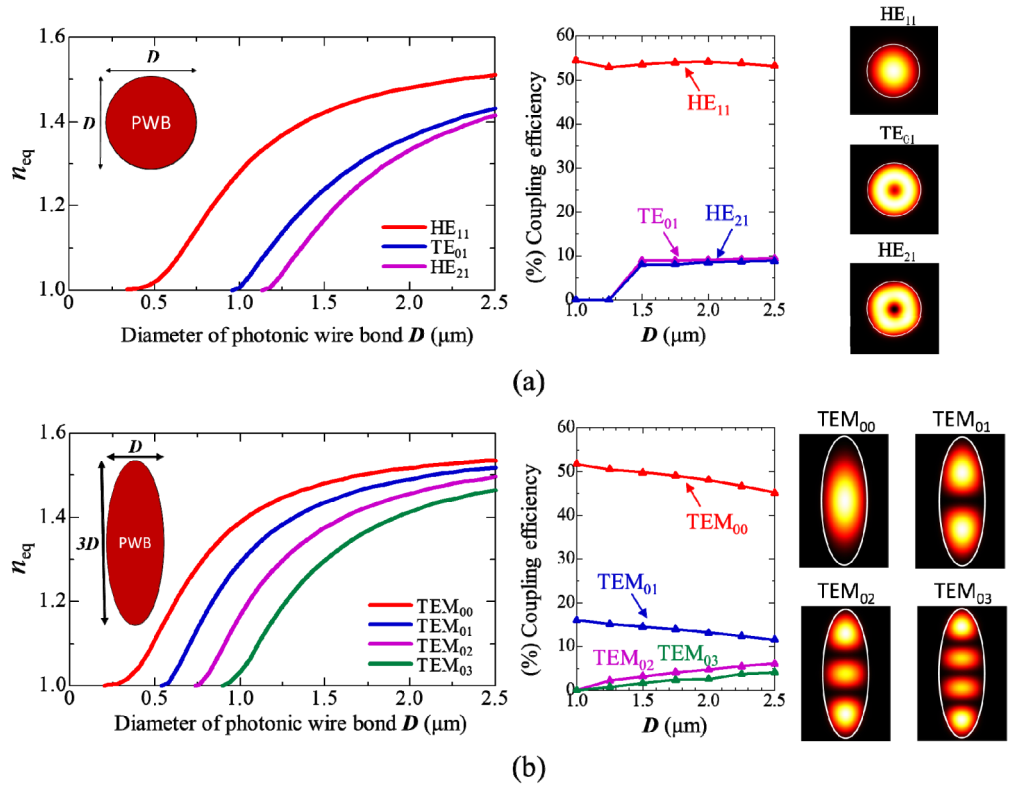

Fig. 2. The calculated equivalent refractive index n_{eq} of several low-order modes as a function of the width of the PWB with aspect ratios of (a) 1:1 and (b) 1:3, the coupling efficiency of each mode in the two types of the PWB to the TE_0 mode of LCI-FP laser and their modal intensity distribution.

#242795 Received 12 Jun 2015; revised 12 Aug 2015; accepted 12 Aug 2015; published 17 Aug 2015

In order to meet the condition of single-mode propagation in the PWB, we proposed a circular cross section similar to the optical fiber and calculated the mode characteristic of the PWB as a function of its diameter; the result indicated that multi-mode propagation could be suppressed when the diameter of the SU-8 wire is less than 1 μm. However, such a small cross section would also weaken the optical confinement in the PWB and degrade the tolerance characteristic during mode coupling between the PWB and optical components. Therefore, the PWB diameter was chosen as a parameter in the calculation of coupling efficiency. The aspect ratio of the PWB cross section is additionally taken into account because of the physical limitation of the focusing spot of the femtosecond laser beam during two-photon lithography. During the fabrication, the laser beam is focused in the volume of SU-8 by using an objective-lens inverted microscope, which can also be used for observing a suspended sample. The PWB is traced out by scanning the focusing spot in three dimensions at high accuracy (60 nm error in Z-axis, 10 nm error in the XY-plane), and the cross-sectional shape mainly depends on the exposure threshold of the photosensitive medium and the numerical aperture (NA) of the adopted objective lens. In our case, the aspect ratio of the PWB was 1:3 after fabrication, which will be explained in the next section.

In the calculation, it is assumed that there is no displacement between the center of the PWB cross section and the core layer of the LCI-FP laser, and we primarily focused on several low-order modes that dominate at higher coupling efficiency. The calculation results with PWBs of aspect ratios of 1:1 and 1:3 are shown in Figs. 2(a) and 2(b), which show the equivalent refractive index n_{eq} as a function of the PWB width for each mode and their coupling efficiencies to the TE_0 mode from the LCI-FP laser. As can be seen in the figure, the PWB modes with 1:1 aspect ratio are labeled as the HE_{11}, TE_{01}, and HE_{21} modes because their modal intensity distributions are nearly the same as those of the conventional step-index fiber. On the other hand, the PWB modes with higher aspect ratios are labeled as the TEM_{00}, TEM_{01}, TEM_{02}, and TEM_{03} modes because their mode profiles are similar to rectangular transverse mode patterns.

According to the calculation result, it becomes more difficult to achieve the single-mode condition with a higher-aspect-ratio PWB. The coupling efficiency between the fundamental modes of PWB and the LCI-FP laser was 55% with 1:1 aspect ratio and 52% with 1:3 aspect ratio when the PWB width was fixed at 1 μm. Large reflection loss is considered a primary reason for the calculated low coupling efficiency because no anti-reflection coating is adopted here, as it cannot be applied to a Fabry–Pérot-type laser in consideration of the light emission. The result is in accordance with our expectation because the intensity distribution of the fundamental modes does not significantly change with the increase in the aspect ratio. The degradation of the coupling efficiency in terms of the PWB width is more evident with a higher aspect ratio. Mode coupling with regard to both types of PWB suffers from the influence of higher-order modes and may interfere with high-speed optical transmission. Some refinement of this tentative end-face-contact coupling structure would be necessary to realize higher efficiency and lower the influence of coupling with higher-order modes.

3. Fabrication

The PWB was formed using high-resolution 3D-lithography technology based on two-photon polymerization, as shown in Fig. 3 [25]. First, the prepared LCI-FP laser and detector chips were roughly mounted on a Si substrate by using BCB adhesive bonding. SU-8 with 200-μm thickness was then spin-coated on the entire surface of the Si substrate and pre-baked. Subsequently, the intense laser beam from a mode-locked Ti-sapphire laser (λ = 800 nm, Δt = 80 fs, f = 82 MHz) was focused in the SU-8 volume by using an objective lens. The SU-8 was cured along the scanning path, which can theoretically be arbitrary according to the control signal from a PC. Finally, the remaining part of the SU-8 was removed by the developer to reveal the cured polymer waveguide.

In order to decrease the influence of higher-order modes and achieve higher coupling efficiency between the PWB and the LCI-FP laser, an appropriate fabrication condition was

#242795 Received 12 Jun 2015; revised 12 Aug 2015; accepted 12 Aug 2015; published 17 Aug 2015

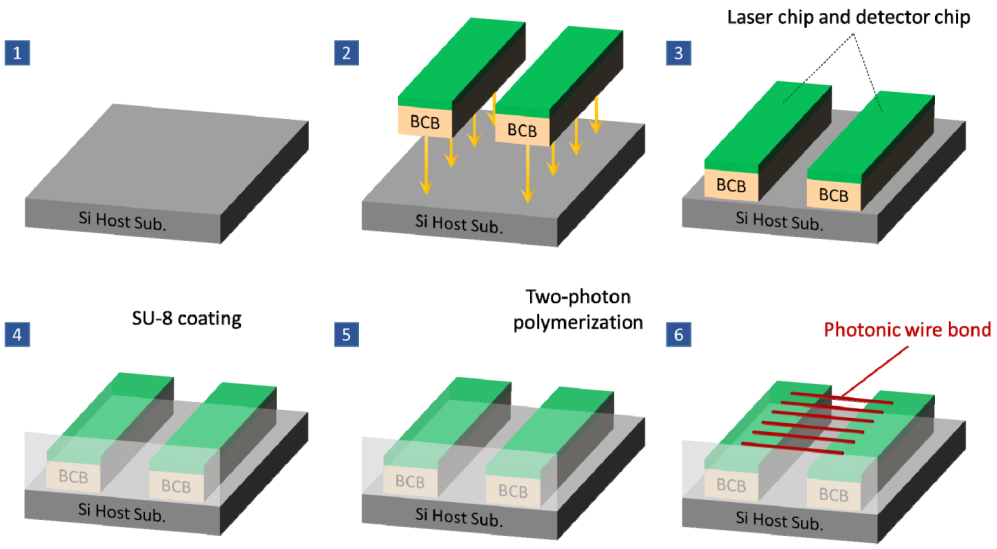

Fig. 3. Process flow for fabricating photonic wire bonding between two optical chips.

required for realizing the PWB with a lower aspect ratio and different width by using an objective lens with a large numerical aperture (NA) and adjusting the exposure dose during two-photon polymerization. The relationship between the PWB width ***D***, average output laser power ***P***, and the scanning speed of the focusing spot ***v*** of the laser beam was calculated according to the following equation [26]:

$$D = \omega_0 \sqrt{\ln \frac{4P^2}{\pi^2 \omega_0^2 v C_{\text{th}}}}, \tag{1}$$

where ω_0 is the $1/e^2$ beam waist at the focal plane and C_{th} is a constant representing the two-photon polymerization threshold of SU-8 in terms of the scanning speed. The beam waist ω_0 can be approximately calculated as follows:

$$\omega_0 = \frac{\lambda}{\pi NA}. \tag{2}$$

During the calculation of the PWB width, C_{th} is fixed at 5.75×10^{-3} mW^2 s/μm^5 as a reference value from [26]; it is believed that this value would not change significantly because the same negative photoresist SU-8 (MicroChem Corp.) was used in this research. The minimum theoretical beam waist ω_0 was first assumed to be 0.5 μm as the NA of the adopted objective lens during the experiment is 0.50. The average laser power varied from 1 mW to 111 mW as the horizontal axis and the scanning speed ***v*** was set to be 10 μm/s in consideration of the experimental conditions. The calculation result is shown in Fig. 4.

To verify the calculation result, PWBs were fabricated on a dummy SOI chip with various average powers of 56, 70, 88, and 111 mW with a fixed scanning speed ***v*** of 10 μm/s. The experimental results are indicated by triangles in Fig. 4. Clear and fine exposure of the SU-8 based on two photon absorption was confirmed when the laser power was above 56 mW. Moreover, intensive thermal damage occurred in SU-8 when the average laser power was 111 mW. Figure 5 shows bird's-eye-view scanning electron microscope (SEM) images of the fabricated PWB. Their width ranges from 1.7 μm to 2.5 μm under different exposure powers.

#242795 Received 12 Jun 2015; revised 12 Aug 2015; accepted 12 Aug 2015; published 17 Aug 2015

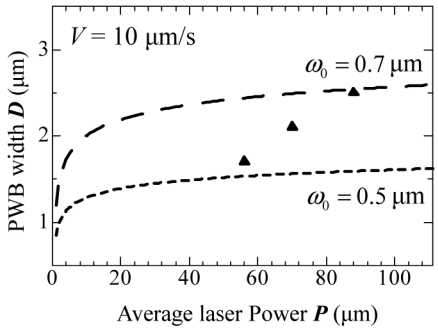

Fig. 4. Calculation result of the PWB width ***D*** in terms of average laser power ***P*** with two values of ω_0 and fixed scanning speed ***v*** = 10 μm/s; the experimental result of the PWB width with fixed scanning speed ***v*** = 10 μm/s in terms of the average laser power.

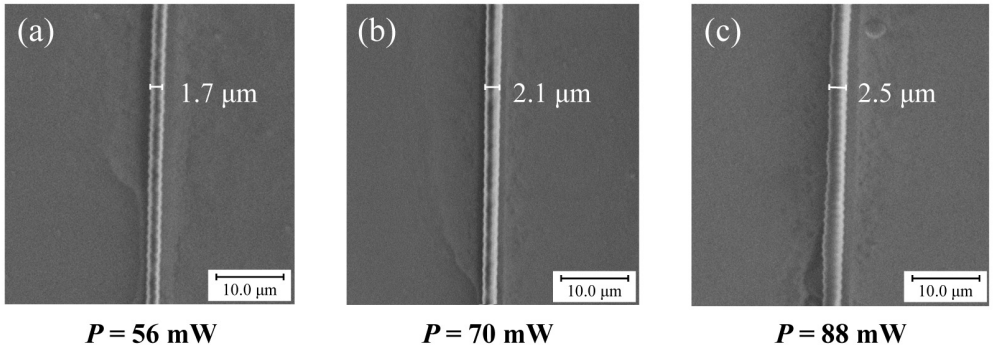

Fig. 5. Scanning electron microscope images of the fabricated PWB with different laser power (a) ***P*** = 56 mW, (b) ***P*** = 70 mW, (c) ***P*** = 88 mW on a dummy SOI chip.

Experimental results did not fit the calculation results in Fig. 4 when the beam waist is assumed to be 0.5 μm. It is suggested that the inconformity is primarily caused by the unevenness of the surface of the SU-8 volume after spin coating on the SOI dummy chip and the surface of the SOI substrate itself, which would lead to an insufficient focusing of the laser beam during the fabrication. The calculation result with the beam waist ω_0 = 0.7 μm is also provided in Fig. 4 for reference, which shows that the diameter of the actual focusing spot is in the range from 0.5 to 0.7 μm. PWBs were also fabricated between two SOI dummy chips for testing the bonding strength between the PWB and optical chips. PWBs with different bonding angles ranging from 0° to 35° were successfully fabricated between two SOI dummy chips under the fabrication conditions of ***P*** = 88 mW and ***v*** = 10 μm/s, as shown in Fig. 6(a). The width of the fabricated PWB is 2.5 μm, which is the same as the former result and is shown in Fig. 6(b). The cross-sectional SEM image of the pier part of the PWB on the SOI chip is shown in the figure. The height of the suspended PWB between two SOI chips is estimated to be two times the height of the part of PWB on the SOI chip because the laser beam was focused on the surface of the chip during two-photon lithography. The dimensions of the pier part of PWB are given as 2.5 μm by 4.0 μm, which indicated that the dimensions of the suspended PWB can be estimated to be 2.5 μm by 8.0 μm. Thus, the aspect ratio of the suspended PWB is considered to be approximately 1:3. Also, the typical amount of surface roughness of the wires provided in the SEM images above was estimated to be 100-200 nm by using critical dimension (CD) measurement. Such surface roughness would indeed introduce measurable scattering loss in the wire bond during long distance transmission. Now we are still working hard on the reduction of the roughness and we believe that it can be achieved by improving the exposure condition in the future work. In the next

#242795 Received 12 Jun 2015; revised 12 Aug 2015; accepted 12 Aug 2015; published 17 Aug 2015

section, the experimental result of the optical transmission between two III-V optical chips through the PWB will be detailed.

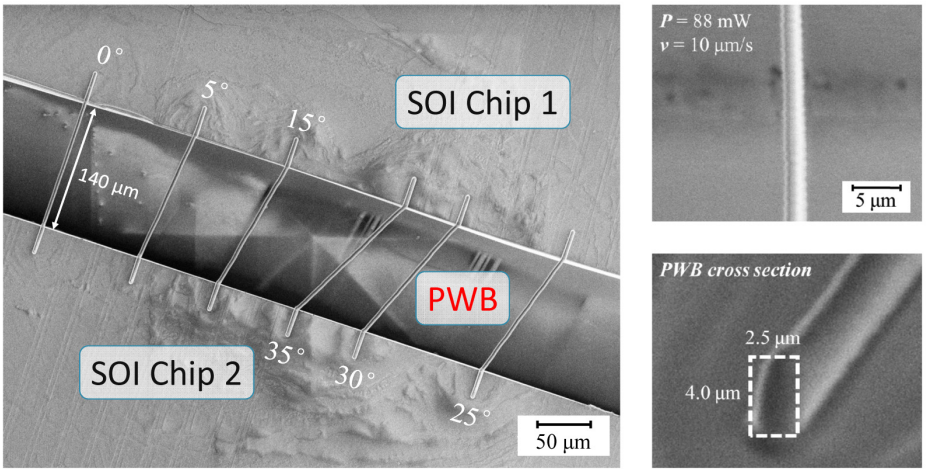

Fig. 6. (a) Two dummy SOI chips connected by PWB with different bonding angles ranging from 0° to 35°. (b) Bird's-eye view of the suspended PWBs between two chips and a cross-sectional image of the pier part of the PWB on the SOI chip taken from an oblique angle by 45 degrees.

4. Experimental result of optical transmission via PWB

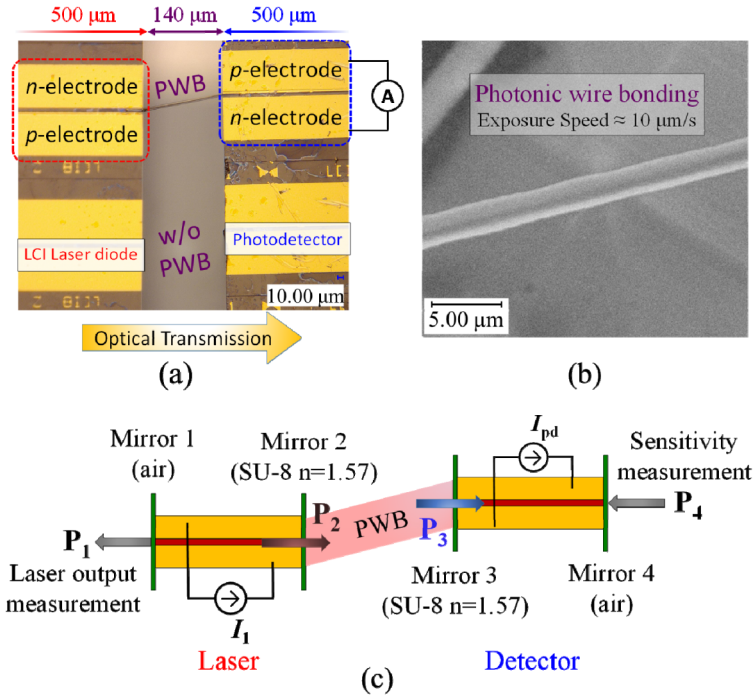

Fig. 7. (a) Optical microscope image of the completed sample. (b) Detailed scanning electron microscope image of PWB. (c) Schematic of optical transmission between the laser and detector chips.

#242795 Received 12 Jun 2015; revised 12 Aug 2015; accepted 12 Aug 2015; published 17 Aug 2015

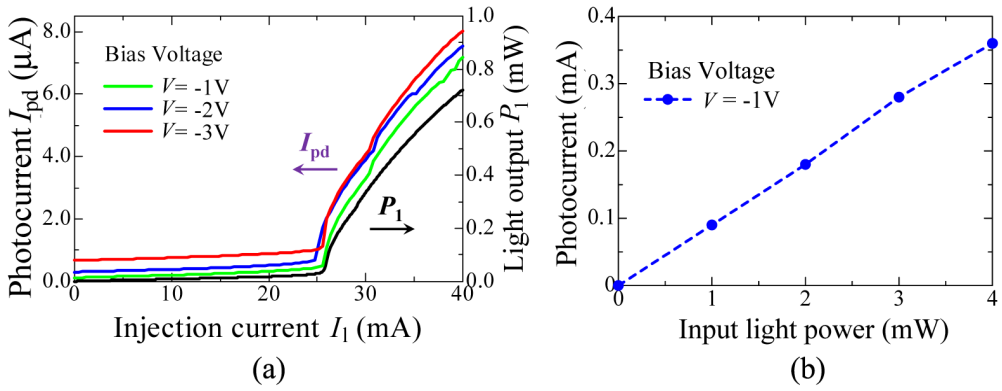

Fig. 8. (a) Measured photocurrent I_{pd} of the detector in terms of the injection current to laser I_1 under different bias voltages. The lasing characteristic of the laser P_1 vs. I_1 is given for reference. (b) Result of photosensitivity measurement of the detector.

The completed sample is shown in Fig. 7(a) together with a detailed view of the PWB in Fig. 7(b). Two III-V LCI optical chips with the same structure were fixed on the Si substrate through BCB adhesive bonding and connected by a 2.5-μm-wide PWB with 1:3 aspect ratio. The relative position of the core layer of the chips was intentionally shifted in the transverse direction by approximately 30 μm in order to confirm the path control of the two-photon lithography and remove stray light during the subsequent optical-transmission experiment. The bonding angle between the PWB and the LCI chips was 10° with a gap of 140 μm between two chips. In order to determine the feasibility of this technology, we first compared the optical-transmission characteristics between the laser and detector chips with and without PWB interconnection. The result shows that with PWB interconnection between the two chips, a photocurrent of 3.0 μA, which is nearly 15 times the detected photocurrent of 220 nA without the PWB interconnection, was detected for an injection current to the laser chip of 30 mA. The noticeable difference in photosensitivity is considered strong proof of the feasibility of the PWB.

The concrete coupling loss between the PWB and laser/detector chips was estimated from the following steps, as illustrated in Fig. 7(c).

(I) The light output P_1 of the LCI-FP laser from the facet without PWB and the photocurrent I_{pd} from the detector were measured with respect to the injection current I_1 with different applied bias voltages. The measurement result is shown in Fig. 8(a). Appropriate optical transmission between the two optical chips is considered to be achieved, because the threshold current of the laser diode is equal to the rising current of the photodiode.

(II) The light output P_2 entering the PWB from the other facet can be theoretically calculated according to the following equation because the ratio of light output from both facets primarily depends on the reflection ratios of the facet mirrors R_1 and R_2 [27], which are 0.27 and 0.11, respectively. Therefore, P_2 is estimated to be approximately two times P_1.

$$P_2 = \frac{(1-R_2)\sqrt{R_1}}{(1-R_1)\sqrt{R_2}} P_1. \tag{3}$$

(III) The photosensitivity of the detector η_{pd} was measured as the incident light P_4 entering the facet without PWB, which is nearly 0.09 A/W according to the result shown in Fig. 8(b).

#242795 Received 12 Jun 2015; revised 12 Aug 2015; accepted 12 Aug 2015; published 17 Aug 2015

(IV) The light power P_3 absorbed by the detector can be estimated through the photocurrent I_{pd} in (I) and photosensitivity of the detector in (III) as follows:

$$P_3 = \frac{I_{pd}}{\eta_{pd}}. \quad (4)$$

(V) The coupling loss between the PWB and the optical chips can eventually be assessed through a comparative analysis of P_2 and P_3 (i.e., $10\log(P_3/P_2)$).

$$\text{PWB loss} = 10\log\frac{P_3}{P_2} \approx 10\log\frac{I_{pd}/\eta_{pd}}{2P_1} \approx 10\text{dB}. \quad (5)$$

As a result, a total coupling loss of approximately 10 dB was estimated, as shown in Eq. (5). The propagation loss of this PWB, which is mainly caused by the material absorption, can be neglected for such a short length because SU-8 is highly transparent at 1550 nm. Thus, the coupling loss between the PWB and laser or detector chips is considered to be roughly 5 dB for each side. Regarding the PWB with 1:3 aspect ratio and 2.5-μm width, the experimental result seems to be consistent to some extent with the calculation result shown in Fig. 2(b), which is nearly 3.5 dB if only the coupling between fundamental modes in PWB and both optical components is considered, because the structure of detector is the same as that of the laser diode. The discrepancy between the simulated and experimental values is considered to be mainly caused by the scattering loss induced by the bonding angle between the PWB and the LCI chips. The coupling loss with the actual structure is recalculated by considering a bonding angle of 10°; the result shows that the coupling loss would increase to 4.5 dB, which is very close to the experimental result. In the future, an anti-reflection coating will be introduced between the PWB and other optical components such as LCI Distributed Feed Back (DFB) lasers for suppressing the reflection loss. Furthermore, the bonding angle of PWB will be reduced by adjusting the scanning path during fabrication for decreasing the impact of scattering. Additionally, reducing the aspect ratio and realizing single-mode propagation in PWB would be other key issues for further enhancing the mode coupling.

5. Summary

In this paper, an emerging technology called photonic wire bonding (PWB) was considered as a promising candidate for realizing high-performance on-chip optical interconnection. We fabricated a 2.5-μm-wide PWB with 1:3 aspect ratio between a GaInAsP/InP LCI-FP laser and detector, which were mounted on a Si substrate using benzocyclobutene adhesive bonding. Appropriate 140-μm optical transmission via PWB was achieved in the experiment, and the total coupling loss between the PWB and optical chips was estimated to be approximately 10 dB. Although the high aspect ratio and propagation of higher-order modes in the PWB remain key issues to be solved for reducing the coupling loss, the feasibility of PWB is considered to be confirmed in the current work; PWBs possess the potential for 3D-freeform combination between different optical components without sacrificing the performance of devices themselves by taking full advantage of two-photon lithography in the field of microfabrication.

Acknowledgments

This work was supported by JSPS KAKENHI Grant Numbers #15H05763, #15J04654, #15J11774, #24246061, #25709026 and #25420321.

#242795 Received 12 Jun 2015; revised 12 Aug 2015; accepted 12 Aug 2015; published 17 Aug 2015